On the northward motion of midlatitude cyclones in a barotropic meandering jet

Ludivine Oruba, Guillaume Lapeyre, Gwendal Rivière

On the Northward Motion of Midlatitude Cyclones in a Barotropic Meandering Jet

LUDIVINE ORUBA AND GUILLAUME LAPEYRE

Laboratoire de Météorologie Dynamique/IPSL, Ecole Normale Supérieure/CNRS/UPMC, Paris, France

GWENDAL RIVIÈRE

CNRM/GAME, Météo-France/CNRS, Toulouse, France

(Manuscript received 10 October 2011, in final form 27 January 2011)

ABSTRACT

The combined effects of the deformation (horizontal stretching and shearing) and nonlinearities on the beta drift of midlatitude cyclones are studied using a barotropic quasigeostrophic model on the beta plane. It is found that, without any background flow, a cyclonic vortex moves more rapidly northward when it is initially strongly stretched along a mostly north–south direction. This meridional stretching is more efficient at forming an anticyclone to the east of the cyclone through Rossby wave radiation. The cyclone–anticyclone couple then forms a nonlinear vortex dipole that propagates mostly northward. The case of a cyclone embedded in uniformly sheared zonal flows is then studied. A cyclone evolving in an anticyclonic shear is stretched more strongly, develops a stronger anticyclone, and moves faster northward than a cyclone embedded in a cyclonic shear, which remains almost isotropic. Similar results are found in the general case of uniformly sheared nonzonal flows.

The evolution of cyclones is also investigated in the case of a more realistic meandering jet whose relative vorticity gradient creates an effective beta and whose deformation field is spatially varying. A statistical study reveals a strong correlation among the cyclone's stretching, the anticyclone strength, and the velocity toward the jet center. These different observations agree with the more idealized cases. Finally, these results provide a rationale for the existence of preferential zones for the jet-crossing phase: that is, the phase when a cyclone crosses a jet from its anticyclonic to its cyclonic side.

1. Introduction

Extratropical surface cyclones are commonly observed to rapidly deepen when they cross the upper-level jet axis from its warm-air to its cold-air side. This was the case for the December 1999 ''Lothar'' storm over Europe (Wernli et al. 2002; Rivière and Joly 2006b) and for most of the storms during the Fronts and Atlantic Storm Track Experiment (FASTEX) campaign (Baehr et al. 1999). Since most cases of the jet-crossing phase occur in the jet exit region, a commonly accepted mechanism for the regeneration phase is dictated by the analogy with the role of the cold left exit region of a jet streak on cyclogenesis. As recalled in the review paper of Uccelini (1990), the decrease in the geostrophic zonal wind in the exit region of a jet streak creates an ageostrophic transverse circulation with ascending motions on the cyclonic side and descending motions on the anticyclonic side. The left exit region of the jet streak (i.e., the exit region on the poleward side) is therefore a favorable region for cyclogenesis. However, as argued by Rivière and Joly (2006a), it is not obvious that this parallel between a jet streak (defined as a maximum wind speed in the total flow) and a large-scale jet stream (defined as a maximum wind speed in the low-frequency flow) is enough to explain the regeneration stage of a surface cyclone in the left exit region of the latter jet. Moreover, in a recent paper, Gilet et al. (2009) have shown the existence of a cyclone regeneration during the crossing phase of a purely zonal baroclinic jet (i.e., without the presence of any transverse circulation). The debate is therefore still open concerning the main mechanism responsible for the regeneration of a surface cyclone crossing the axis of a large-scale jet. In parallel with the question of the regeneration process, another important issue of the jet-crossing phase concerns the

Corresponding author address: Guillaume Lapeyre, LMD/IPSL, Ecole Normale Supérieure, 24 Rue Lhomond, 75005 Paris, France.
E-mail: glapeyre@lmd.ens.fr

DOI: 10.1175/JAS-D-11-0267.1

identification of the key factors influencing the motion of a surface cyclone perpendicular to the jet axis. In a barotropic context on the sphere, Rivière (2008) showed evidence of the role played by the combined effects of the horizontal deformation of the background flow and the nonlinearities in determining the motion of a cyclonic vortex but did not identify the associated mechanism, which is the purpose of the present study.

The role of the horizontal deformation tensor in the development of midlatitude surface cyclones was previously studied in the literature, including the effects of its shearing component (e.g., James 1987; Davies et al. 1991; Thorncroft et al. 1993) and its stretching component (e.g., Cai and Mak 1990; Schultz et al. 1998). Davies et al. (1991) have studied the sensitivity of the growth rate and the structure of the most unstable modes to the sign and intensity of the horizontal shear in a baroclinic jet–like flow. The modes have weaker growth rates and their structures are modified in presence of the shear. During the nonlinear development, their structural changes increase, leading to different kinds of fronts according to the shear properties. Starting from similar frameworks but initializing the perturbation with isolated vortices, it has been shown that the Bergen (Bjerknes and Solberg 1922) cyclone model applies more to cyclones evolving within a cyclonic background shear (Wernli et al. 1998) or a diffluent zone (Schultz et al. 1998). On the contrary, the model of Shapiro and Keyser (1990) fits more with cyclones embedded in a confluent flow (Schultz et al. 1998). Note finally that the meridional motion of the cyclones has never been systematically studied in the atmospheric midlatitude context.

In the context of geophysical fluid dynamics (GFD), the effect of the horizontal deformation on vortices has been analyzed in numerous papers. Kida (1981) studied the exact solutions for an idealized elliptical vortex (with uniform vorticity) evolving in a background flow having both strain and vorticity components. The background replaces, in first approximation, the effect of other vortices or a large-scale jet. Dritschel (1990) studied the stability of elliptical patches of uniform vorticity in a flow with uniform strain and rotation. He showed that instability appears for high enough strain rates. Legras and Dritschel (1993) studied numerically the behavior of a vortex whose vorticity is not uniform. They showed that stripping erodes the exterior of the vortex and generates high vorticity gradients at the edge of the vortex. Trieling et al. (1998) investigated both experimentally and theoretically the evolution characteristics of dipolar vortices in a strain flow. Depending on the initial orientation of the dipole, they observed either a head–tail structure or a pair of elliptic-like monopolar vortices.

In this context, Gilet et al. (2009) revisited the GFD results on the vortex shape evolution and extended them to a baroclinic two-layer atmosphere. In a background flow composed of uniform vertical and horizontal shears, they showed that the vortex shape depends strongly on the sign of the horizontal shear: in an anticyclonic shear, a cyclonic vortex is stretched strongly whereas it remains quasi-isotropic in a cyclonic shear. They also showed that the trajectory of the surface cyclone depends on the vertically averaged meridional PV gradient (verified in a more realistic background flow with a meridionally confined zonal jet), that is, the so-called effective β. Thus, both the horizontal shear and the effective β seem essential for the jet crossing and the deepening of cyclones.

The role of β (the meridional gradient of the Coriolis parameter) in the motion of vortices is well known in oceanography and tropical cyclone literature. This concept was introduced in oceanography by McWilliams and Flierl (1979) for oceanic rings. They focused on the combined effects of β and nonlinearities in a quasigeostrophic regime. They underlined a westward linear propagation motion of the vortex, leaving behind a weak Rossby wave wake, due to β Rossby waves. For a cyclonic (anticyclonic) vortex, the dispersion pattern initially consists of a positive (negative) center of potential vorticity to the west of the vortex and a negative (positive) one to the east (these centers are called gyres). For significant nonlinearities, a northward (southward) motion of the vortex is also observed: the leading and trailing dispersion centers have secondary circulations that both act to advect the main vortex northward (southward). The steering of the primary vortex by β-induced asymmetric gyres (the β gyres) is called the β drift. The interaction of this effect with a zonal Rossby wave that modifies the background potential vorticity field was studied by Sutyrin and Carton (2006). The β drift, combined with the effect of the environmental flow, was also studied for tropical cyclones (Holland 1983, and references therein). More specifically, it was shown that sheared flows could accelerate or decelerate the beta drift depending on its cyclonic/anticyclonic nature (Ulrich and Smith 1991; Williams and Chan 1994; Li and Wang 1996; Wang et al. 1997).

The role of horizontal deformation of the environmental flow and of the β drift is often overlooked to explain the life cycle of surface cyclones. In the present paper, these processes will be examined in a midlatitude context by performing idealized numerical simulations of a barotropic model. We leave to future work the baroclinic case where the goal is to reproduce and analyze the jet-crossing phase of surface midlatitude cyclones. Note that only the evolution of finite-amplitude

perturbations is analyzed here and considerations on the genesis of synoptic perturbations are beyond the scope of the present study. Section 2 describes the barotropic model and provides information on the large-scale background flow and the perturbation initialized in the model, the latter being reduced to a vortex. In section 3, simulations of the beta drift of an elliptic vortex with no background flow are presented. The combined effects of uniform shears and β on the vortex trajectory are studied in section 4. Section 5 is dedicated to the evolution of cyclones in a barotropic meandering large-scale jet and a rationale for the existence of preferential zones of the jet-crossing phase is provided. Finally, our conclusions are given in section 6.

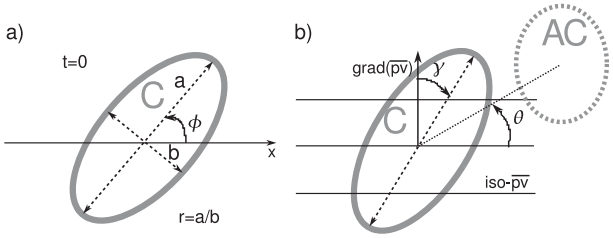

FIG. 1. (a) Definition of parameters used in the text concerning an initial cyclone satisfying Eq. (4). Parameters a and b are respectively the semimajor and semiminor axes of the ellipse, r is the aspect ratio, and ϕ is the angle of the great axis with the x axis. (b) Parameters for a cyclone: γ is the angle of the great axis with the large-scale potential vorticity gradient, and θ is the angle between the axis formed by the centers of the cyclone and anticyclone with the x axis.

2. The numerical framework

a. The barotropic model

We consider a barotropic model of the atmosphere on a β plane. The model consists in integrating the potential vorticity (PV) q, defined as

$$q = \nabla^2\psi + f_0 + \beta y, \tag{1}$$

where f_0 is the Coriolis parameter, β is its meridional derivative, and ψ is the velocity streamfunction. The flow is separated into a large-scale background flow, denoted with bars and maintained stationary, and a perturbation denoted with primes such that

$$q(x, y, t) = \overline{q}(x, y) + q'(x, y, t). \tag{2}$$

The evolution equation of the PV perturbation q' is

$$\frac{\partial q'}{\partial t} + \overline{\mathbf{u}} \cdot \nabla q' + \mathbf{u}' \cdot \nabla \overline{q} + \mathbf{u}' \cdot \nabla q' = 0, \tag{3}$$

where $\mathbf{u} = (u, v)$ designates the geostrophic wind. The decomposition (2) can be thought of as a decomposition into a low-frequency $\overline{q}$ and a high-frequency part q' (corresponding to the synoptic perturbation). Here it is assumed that the high frequencies do not affect the low frequencies. The horizontal domain is biperiodic, and we integrate Eq. (3) using a pseudospectral model with biharmonic diffusion.

b. The initial conditions

The initial conditions are composed of a background flow that is described in each section and a localized perturbation. The perturbation is an elliptic vortex whose relative vorticity is defined as

$$\zeta'(x, y) = A \exp\left\{ -\left[\frac{(x\cos\phi + y\sin\phi)^2}{L_0^2(1 - e^2)} + \frac{(-x\sin\phi + y\cos\phi)^2}{L_0^2} \right] \right\}. \tag{4}$$

Parameters e and ϕ designate the eccentricity and the tilt with the x axis of the ellipse, and $A > 0$ is the relative vorticity amplitude of the perturbation. The semimajor axis of the ellipse has a length L_0 while the semiminor axis length is $L_0\sqrt{1 - e^2}$ (see Fig. 1a).

Other parameters are introduced in Fig. 1b. Note that γ is the angle of the major axis of the cyclone (in term of relative vorticity) with the local potential vorticity gradient of the large-scale flow. When only β is considered, the PV gradient points northward and the initial value of γ is $\gamma_0 = \gamma(t = 0) = \phi - 90°$. Also, r is the aspect ratio of the elliptic cyclone (i.e., the ratio between the major and minor radii of the ellipse). It is initially equal to $r_0 = r(t = 0) = 1/\sqrt{1 - e^2}$. These two parameters ($r$ and γ) will vary as a function of time and will be estimated by diagonalizing the inertia matrix of the perturbation relative vorticity (keeping the 40 points where vorticity is the greatest): supposing the cyclone shape is an ellipse, the eigenvalues are the semiminor and semimajor axes and eigenvectors give the direction of the ellipse axis.

3. No background flow

a. The experimental design

In this section, we consider the simple case of no background flow ($\overline{u} = 0$ and $\partial_y \overline{q} = \beta$). We choose $\beta = 4.8 \times 10^{-11}$ m^{-1} s^{-1} (i.e., 3 times the common values in the midlatitudes) to get a more rapid distinction between the different behaviors of the cyclones. Another reason is based on the fact that in the midlatitudes, an effective

beta effect exists because of the meridionally confined jet, which tends to increase the effect of the variations of the Coriolis parameter. The domain size is $L_x = L_y =$ 16 000 km. The spatial and temporal resolutions are equal to $\Delta x = \Delta y = 62.5$ km and $\Delta T = 112$ s.

To define the perturbation ζ', we need to set parameters A and L_0 in Eq. (4). In the classical theory of the β drift, the cyclone generates two gyres (a cyclonic one to its west and an anticyclonic one to its east) that displace it northward. The gyres are due to the term $\mathbf{u}' \cdot \nabla\overline{q} = \beta v'$ in Eq. (3). The simplest way to look at the sensitivity of the vortex trajectory to the initial orientation of the vortex is to modify the initial tilt of the vortex with the x axis, keeping all the other parameters unchanged. However, the result would be too straightforward. A south–north-oriented vortex would lead to larger $v' = \partial_x\psi'$ and stronger beta gyres than a west–east-oriented vortex and would move more rapidly poleward. A more relevant alternative is to keep the maxima of the relative vorticity ζ' and the meridional velocity v' the same when modifying e and ϕ. To do this, for a given A, we calculate L_0 in such a way that $\max(v')$ is maintained the same thanks to a numerical procedure based on dichotomy. The parameters we choose for the cyclones are such that $\max(\zeta') = 1.5 \times 10^{-4}$ s^{-1} and $\max(v') = 22$ m s^{-1}. The typical associated length scale L_0 is around 460 km.

b. Results

We first examine the time evolution of three vortices having different configurations, one axisymmetric with $e = 0$, and two elliptic with $e = 0.96$ (corresponding to an aspect ratio around 3.6) but with different initial angles with the PV gradient: $\gamma_0 = 45°$ and $\gamma_0 = -45°$.

Figure 2 shows the relative vorticity field of these three vortices at different times. In all cases, the cyclone moves northwestward consistently with the combined effects of the linear and nonlinear β terms (McWilliams and Flierl 1979). This is illustrated by the presence of the β gyres, the effect of which can be detected through the existence of an anticyclone to the east of each cyclone (see Figs. 2d–f). In the first few hours, the northward motion of the cyclone is the same for all cases (Fig. 3a). For each cyclone, the anticyclonic perturbation developing to the east of the cyclone tends to amplify and rotates cyclonically around the cyclone (see Figs. 2g–i). Once the anticyclone is big enough, an asymmetric vortex dipole propagates: the nearby cyclone and anticyclone advect each other as two coherent structures (see Fig. 2i). The propagation is mainly perpendicular to the axis joining the cyclone to the anticyclone. In this situation, we cannot call this a β gyre since strong nonlinearities arise and this departs from the standard picture.

The difference in behavior of the two initially stretched cyclones can be explained by examining their time evolution: both cyclones self-rotate cyclonically in time (left and right columns of Fig. 2) and advect the anticyclones parallel to their major axis. The cyclone with $\gamma_0 = 45°$ mainly advects northeastward the anticyclone that is initially created on its eastern side. The anticyclone is thus first located to the northeast of the cyclone (Fig. 2d) and then mainly to the north because the cyclone major axis self-rotates cyclonically (Fig. 2g). This location is not efficient for the anticyclone intensification because it is not reinforced by the generation of the Rossby wave, which is essentially oriented eastward. Since the anticyclone is weaker than the cyclone, it is more advected by the cyclone than the reverse, and the vortex dipole will move more westward than northward as observed in Fig. 2g. On the contrary, for the cyclone with $\gamma_0 = -45°$, the anticyclone also follows the rotation of the cyclone but remains almost to the east of the cyclone since the cyclone turns its orientation along the north–south direction. In that case, the anticyclone is continuously reinforced by the generation of the Rossby wave to the east of the cyclone (see Figs. 2f,i). As the anticyclone has a large amplitude and is almost east of the cyclone, the vortex dipole has a strong northward component (Fig. 2i).

The northward motion sensitivity to the tilt γ_0 is now examined using $e = 0.96$ and γ_0 varying from $-45°$ to 90° every 45°. Figure 3a shows the evolution of the meridional position of these cyclones with time. For comparison, we added the axisymmetric cyclone results. We observe that a stretched cyclone with $\gamma_0 \in [0, -45°]$ moves northward (in the $\overline{q}$-gradient direction) more quickly than the other ones.

Figure 3b shows the ratio of the minimum of relative vorticity (absolute value) to its maximum versus time for different γ_0. This quantity helps to determine the anticyclone strength and the potential for a vortex dipole to exist (assuming that the cyclone strength is fixed). Deformed cyclones with $\gamma_0 \in [0, -45°]$ have a stronger anticyclone (compared to the cyclone) than the other ones. Simulations including only linear terms exhibit the same qualitative picture (Fig. 3c): the cyclone with $\gamma_0 = 0$ has a stronger anticyclone than those with $\gamma_0 = 45°$ and $\gamma_0 = -45°$. These three cyclones have a stronger anticyclone than the axisymmetric cyclone. The zonally stretched case ($\gamma_0 = 90°$) is the one having the weaker anticyclone.

We can now examine the dependence of the northward motion and the strength of the anticyclone on the initial aspect ratio $r_0 = 1/\sqrt{1 - e^2}$ of the cyclone for the most efficient initial tilt ($\gamma_0 = 0°$). Figure 4a shows at different times that the northward motion (as diagnosed

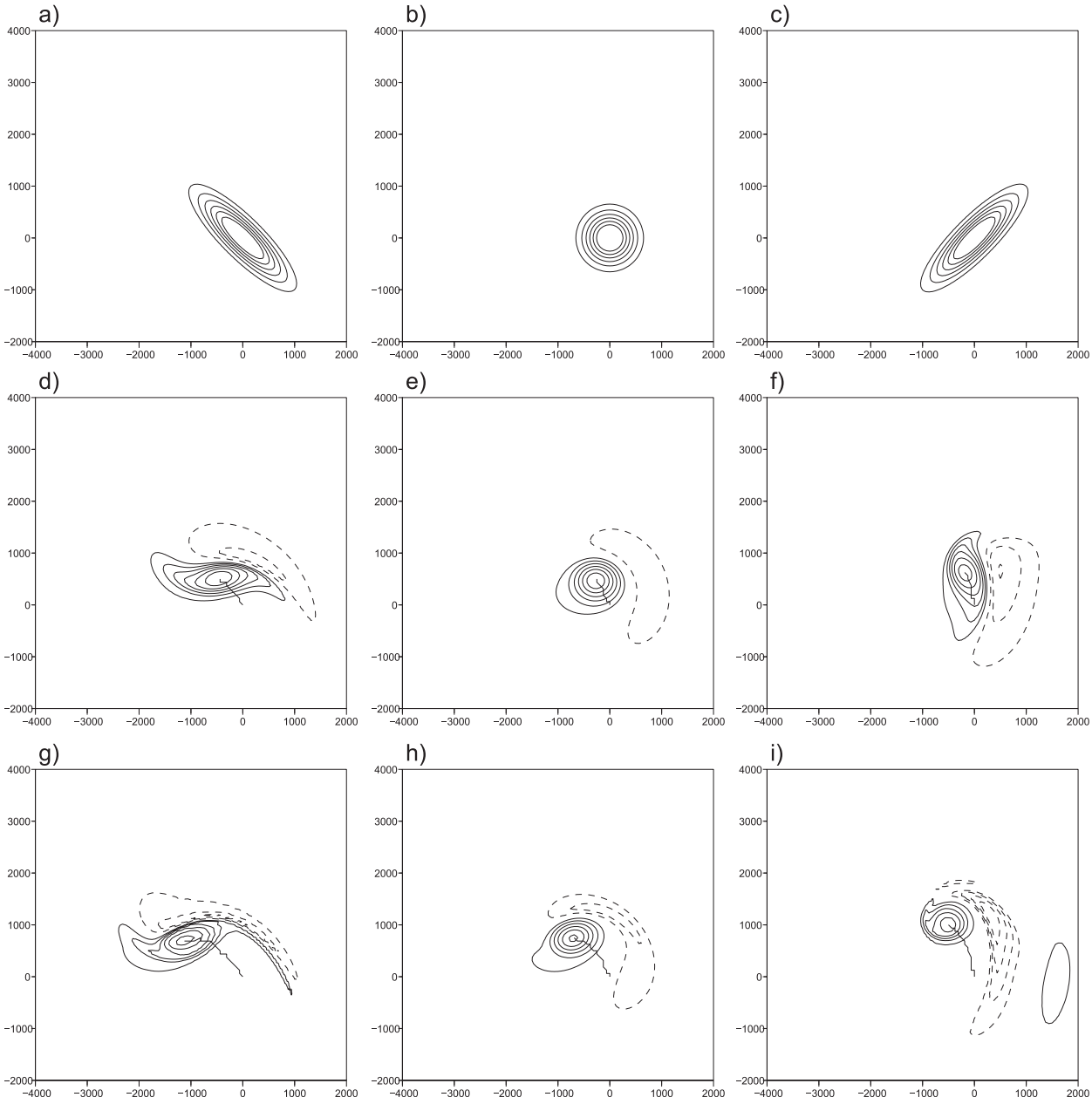

FIG. 2. Relative vorticity field at different times for a cyclone with (a),(d),(g) $e = 0.96$ and $\gamma_0 = 45°$, (b),(e),(h) $e = 0$, and (c),(f),(i) $e = 0.96$ and $\gamma_0 = -45°$, where (a)–(c) $t = 0$ h, (d)–(f) $t = 15$ h, and (g)–(i) $t = 30$ h. Positive values are represented by solid contours between 2×10^{-5} and 1.1×10^{-4} every 1.8×10^{-5} s^{-1}. Negative values are represented by dashed contours between -1.1×10^{-4} and -2×10^{-5} s^{-1} every 1.8×10^{-5} s^{-1}. The thick black line is the trajectory of the cyclone.

by the meridional position) of the cyclone is strongly affected by its elongation: an elongated cyclone moves northward more rapidly than a less elongated one. The relative amplitude of the anticyclone compared to the cyclone (measured as the absolute ratio of the minimum relative vorticity of the perturbation to its maximum) at different times is shown in Fig. 4b: the more deformed the cyclone, the stronger the anticyclone. A similar result holds for the corresponding linear experiments (Fig. 4c), except that there is a plateau when $r_0 > 4.5$. Thus a linear process ensures a stronger anticyclone for a more elongated cyclone. A qualitative interpretation of this observation is provided below in terms of the group velocity of Rossby waves.

To conclude, both the angle γ_0 and the aspect ratio of the cyclone play a role in the anticyclone growth. As

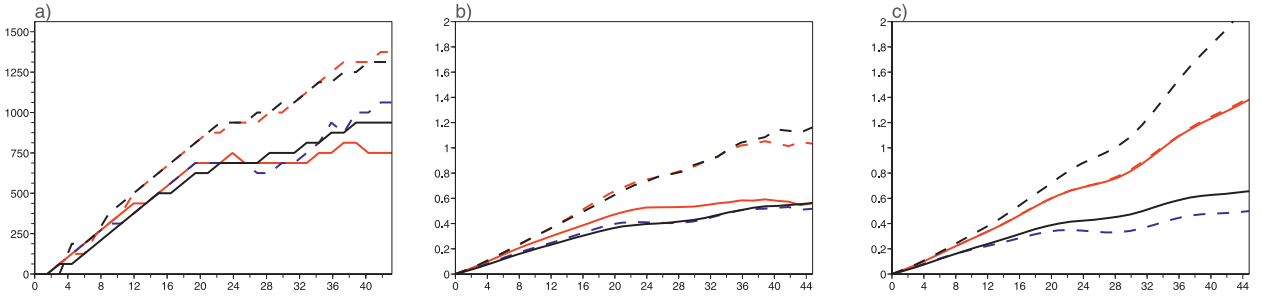

FIG. 3. (a) Meridional position (km) of the different cyclones as function of time (h). (b),(c) Ratio of the minimum of the perturbation relative vorticity to its maximum in the (b) nonlinear and (c) linear experiments as a function of time. The solid black line corresponds to $e = 0$. Other lines correspond to the vortex with $e = 0.96$: solid red line with $\gamma_0 = 45°$, blue line with $\gamma_0 = 90°$, dashed red line with $\gamma_0 = -45$, and dashed black line with $\gamma_0 = 0°$.

γ_0 gets closer to 0° (in a linear context) or to [−45°, 0°] (in a nonlinear context), the anticyclone becomes stronger, and the cyclone moves faster northward. In addition, the more meridionally stretched the cyclone is, the stronger the anticyclone (due to linear effects) and the more rapid the northward displacement of the cyclone. We made sensitivity tests changing the cyclone initial shape (for instance, a vortex Gaussian in streamfunction) or changing the amplitude and the results do not qualitatively change.

c. *Interpretation*

We now analyze the linear process, which ensures a stronger anticyclone when the cyclone is more stretched along a direction near $\gamma = 0°$. In the linear simulation, only the radiation of Rossby waves matters. The relation between the meridional wind and the relative vorticity in Fourier space is $\hat{v}' = -ik\hat{\zeta}'/K^2$, where k, l, and K denote respectively the zonal, meridional, and total wavenumbers. In our simulations, since the maxima of v' and ζ' are kept the same when changing the eccentricity and the tilt, the ratio k/K^2 remains the same, too. Let us now consider the conservation of wave activity,

$$\partial_t \mathcal{A} + \partial_x(c_g^x \mathcal{A}) = 0, \tag{5}$$

where $\mathcal{A} = \langle \zeta'^2 \rangle_y/(2\beta)$ is the wave activity density, $\langle \cdot \rangle_y$ the meridional average, and c_g^x the zonal group velocity. If we introduce the zonal phase speed c^x, we obtain

$$\partial_t \mathcal{A} + \partial_x(c^x \mathcal{A}) = -\partial_x[(c_g^x - c^x)\mathcal{A}]. \tag{6}$$

The dispersion of the wave is quantified by the right-hand side term of Eq. (6). The group velocity is equal to $c_g^x = (k^2 - l^2)\beta/K^4$ and the phase velocity is $c^x = -\beta/K^2$. It leads to $c_g^x - c^x = 2k^2\beta/K^4$, which is the same between the different experiments at the initial time. The value of $\mathcal{A}$ is the same, too, because $\max(\zeta')$ is fixed, and $(c_g^x - c^x)\mathcal{A}$ is therefore the same. Only the dispersion term $\partial_x[(c_g^x - c^x)\mathcal{A}]$ varies with k. The greater k is, the greater $\partial_x[(c_g^x - c^x)\mathcal{A}]$ and the stronger the anticyclone.

The quantities $-\partial_x[(c_g^x - c^x)\mathcal{A}]$ and $-(c_g^x - c^x)\mathcal{A}$ are shown for three different elongated cyclones ($e = 0$, $e = 0.8$, and $e = 0.9$) in Fig. 5. They are estimated by computing respectively $[\partial_t \zeta'^2 + \partial_x(c^x \zeta'^2)]/(2\beta)$ and its integral with respect to x for $y = 0$ with c^x approximated by $\beta \min(\psi')/\max(\zeta')$. As expected, $-(c_g^x - c^x)\mathcal{A}$ (Fig. 5a) has the same amplitude for the three cases and

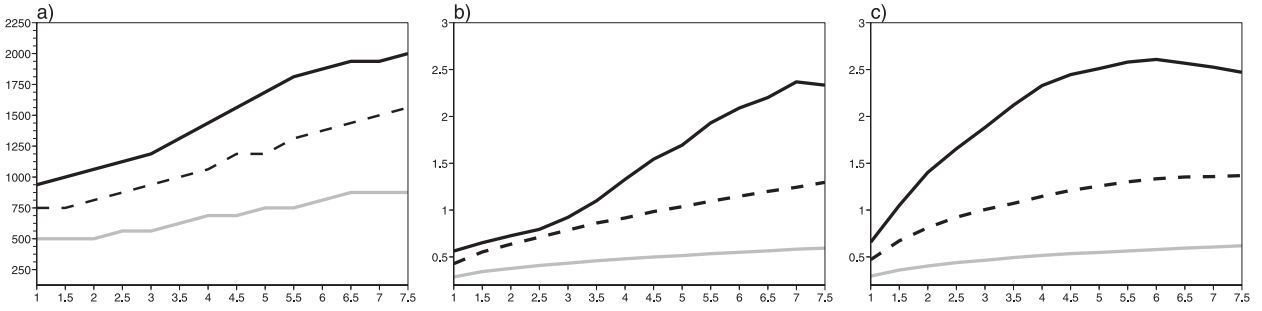

FIG. 4. (a) Meridional position (km) at different times of the different cyclones for different r_0 (in abscissa) and $\gamma_0 = 0°$. (b),(c) Ratio of the minimum of the perturbation relative vorticity to its maximum in the (b) nonlinear and (c) corresponding linear experiments for different r_0. Lines correspond to $t = 14.9$ (gray), 29.9 (dashed black), and 44.8 h (solid black).

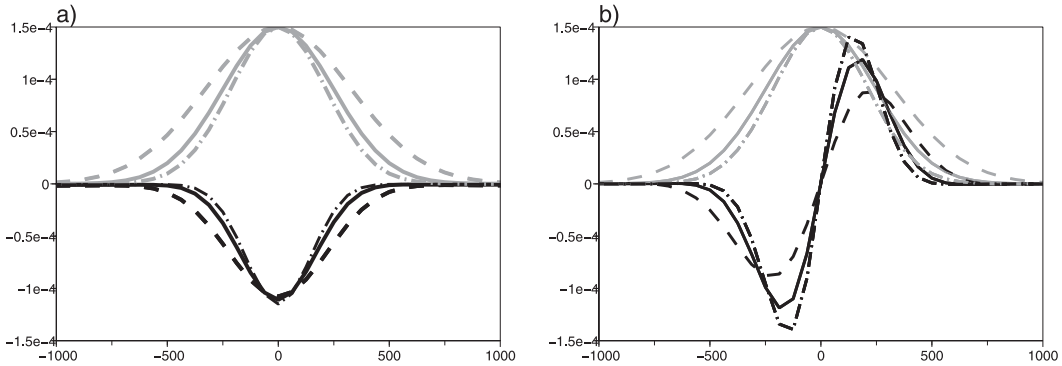

FIG. 5. Shown in gray are initial vorticity profiles vs x (km) at $y = 0$ km for a cyclone, with $e = 0$ (dash-dotted), $e = 0.8$ (solid), and $e = 0.9$ (dashed). In black are estimations of (a) $-(c_g^x - c^x)\mathcal{A}$ and (b) $-\partial_x[(c_g^x - c^x)\mathcal{A}]$.

$-\partial_x[(c_g^x - c^x)\mathcal{A}]$ depends on the case. The latter term is stronger for $e = 0.9$ and decreases with e (Fig. 5b). It is coherent with the results of Fig. 4c. It is also consistent with the fact that $\partial_x[(c_g^x - c^x)\mathcal{A}]$ varies with k. Indeed, it has been checked numerically that the quantity $\max(v')/\min(\psi')$ that approximates k increases with e [$\max(v')$ is unchanged but $\min(\psi')$ decreases when e increases]. Therefore, a more stretched cyclone along the y direction has a greater k that renders larger the dispersion term of Eq. (6). It explains why for $\gamma = 0$, the anticyclone is stronger for a greater aspect ratio r in the linear simulations (see Fig. 4c). This first-order interpretation based on Rossby wave radiation for different cyclone shapes clearly indicates that the generation of an anticyclone east of the cyclone is even more important as the cyclone is meridionally stretched, which confirms the numerical findings of the previous section.

4. Effect of a linear deformation field on a cyclone drift

a. Notion of effective deformation

As seen previously, an elongated cyclone moves more rapidly northward than an axisymmetric one. It is due to the development of an anticyclone to its east (through the β effect), the amplitude of which is comparable to the cyclone, so that they form a vortex dipole. It is relevant to examine a more general case for which the large-scale background flow will force the elongation of the cyclone.

The characteristics of a velocity field $\overline{\mathbf{u}} = [\overline{u}(x, y), \overline{v}(x, y)]$ in terms of stretching and shearing can be described by its deformation magnitude $\overline{D}$

$$\overline{D} = \sqrt{\left(\frac{\partial \overline{v}}{\partial x} + \frac{\partial \overline{u}}{\partial y}\right)^2 + \left(\frac{\partial \overline{u}}{\partial x} - \frac{\partial \overline{v}}{\partial y}\right)^2}, \tag{7}$$

its relative vorticity $\overline{\zeta}$

$$\overline{\zeta} = \frac{\partial \overline{v}}{\partial x} - \frac{\partial \overline{u}}{\partial y}, \tag{8}$$

and the Okubo–Weiss criterion Δ (Okubo 1970; Weiss 1991),

$$\Delta = \overline{D}^2 - \overline{\zeta}^2. \tag{9}$$

From a meteorological point of view, Rivière and Joly (2006a) have called Δ the effective deformation since it is related to the low-frequency or the stationary background wind $\overline{\mathbf{u}}$, and not to the total flow $\overline{\mathbf{u}} + \mathbf{u}'$. The quantity $\overline{D}$ characterizes the straining effects that tend to elongate any perturbation. On the contrary, $\overline{\zeta}$ represents the rotation effect that makes any perturbation rotate over itself. When $\Delta > 0$, the straining effects dominate the rotation and the perturbation will be stretched. When $\Delta < 0$, the rotation effect dominates and the perturbation will not be elongated very much. Note that Lapeyre et al. (1999) have proposed a modified version of the Okubo–Weiss criterion to take into account its non-Galilean invariance (and the rotation of the strain axis).

b. The experimental design

The time evolution of a vortex in different large-scale flows having uniform shears is examined in the present section. The potential vorticity gradient is still northward as it is due only to the β effect ($\beta = 4.8 \times 10^{-11}$ $\mathrm{m^{-1}\ s^{-1}}$ as in the last section). The background velocity components have linear profiles that can be expressed as

$$\overline{u}(x, y) = -\frac{U}{a} c_y y,$$
$$\overline{v}(x, y) = \frac{U}{a} c_x x, \tag{10}$$

where U is a velocity scale (here $U = 48$ m s^{-1}), a is a length scale ($a = 2000$ km), and c_x and c_y are constant in space and time. The stretching characteristics of this flow are $\overline{D} = (U/a)|c_x - c_y|$, $\overline{\zeta} = (U/a)(c_x + c_y)$, and $\Delta = -4(U^2/a^2)c_x c_y$. This means that for $c_x c_y > 0$ the flow will be dominated by rotation, and for $c_x c_y < 0$ by deformation. The appendix describes how to create a velocity field such as Eq. (10) in a biperiodic domain of size $L_x = L_y = 16\,000$ km. The spatial and temporal resolutions for numerical integrations are equal to $\Delta x = \Delta y = 62.5$ km and $\Delta T = 112$ s.

c. Purely zonal large-scale flow

The first case considered is a meridionally sheared zonal flow for which $c_x = 0$, so that $\overline{u}(x, y) = -(U/a)c_y y$ and $\overline{v}(x, y) = 0$. In this case, the rotation and the deformation are equal in absolute value leading to $\Delta = 0$. A positive value of c_y corresponds to a cyclonic shear ($\overline{\zeta} = c_y U/a > 0$) whereas a negative one corresponds to an anticyclonic shear $\overline{\zeta} < 0$. The cyclonic and anticyclonic shear cases will be hereafter denoted as C and A, respectively. Note that the two linear terms of Eq. (3) are both responsible for a motion along the x axis and do not distort the northward motion caused by the nonlinear term. Initial cyclones are axisymmetric [as defined in Eq. (4) with $e = 0$] and are located in the center of the domain. Their parameters are $\max(\zeta') = 1.5 \times 10^{-4}$ s^{-1} and $\max(v') = 22$ m s^{-1}, corresponding to $L_0 \approx 460$ km.

Gilet et al. (2009) have shown that in a purely zonal large-scale flow (as the one considered here) and in the absence of the beta effect, an initially axisymmetric cyclone evolving in a cyclonic shear remains almost axisymmetric whereas it keeps stretching when it is embedded in an anticyclonic shear. As explained by Kida (1981) and Dritschel (1990), who examined the effect of a linear velocity field on a vortex patch of uniform relative vorticity, the deformation of a vortex depends on the rotational effect due to both the background vorticity and the vortex and on the deformation of the background flow (the deformation induced by the vortex does not apply to itself). In C, the vorticities of the background flow and the vortex have the same sign that tend to concur against the deformation of the background flow. In such a rotation-dominated regime, the vortex cannot be stretched. On the other hand, in A, the two rotational effects tend to cancel each other, so that the deformation is more able to dominate.

Figure 6 shows the relative vorticity of the perturbation at different times in C and A for $|c_y| = 0.5$. After 51 h, the cyclone in C (Fig. 6c) remains almost axisymmetric whereas the cyclone in A is stretched (Fig. 6f). We note that this difference of stretching is not visible after 30 h, which is due to a transient contraction and stretching of the axisymmetric vortex in a shear, as explained in Kida (1981). In both shears, the vortices first move toward the northwest (Figs. 6a,d). After 15 h, the cyclone in C deviates and moves mostly westward (Figs. 6b,c) whereas the cyclone in A still moves northward for a while (Fig. 6e) and later northeastward (Fig. 6f). We observe that the anticyclone intensifies less in C than in A. After 15 h, the anticyclone is located to the northeast of the cyclone in C (Fig. 6a) and then rotates cyclonically around the cyclone. A vortex dipole is not clear in that case (Fig. 6c), while it is obvious in A (Fig. 6f). In the latter case, after 15 h, the anticyclone is located to the east of the cyclone, with a similar amplitude as in C at the same time. However, it strongly intensifies reaching an amplitude similar to the cyclone (in terms of vorticity) at 30 h and is maintained on the eastern side of the cyclone. This is a favorable situation for its amplification through Rossby wave radiation. After 30 h, it forms a vortex dipole with the cyclone and they both move northeastward (Figs. 6e,f).

Figures 7a and 7b respectively quantify the stretching r and the angle of the cyclone orientation γ with respect to the PV gradient as function of time (see the end of section 2b for their computation). In C, the aspect ratio of the cyclone does not exceed the value 1.8 and the vortex keeps rotating anticlockwise (Figs. 7a,b). In A, the aspect ratio is larger than in C after 34 h and reaches 2.6 at $t = 54$ h (Fig. 7a). Furthermore, the tilt with the PV gradient γ reaches a stable value near $-40°$ (Fig. 7b). There is a transient period during the first 34 h when cyclones have a similar stretching. This period was much shorter in the study of Gilet et al. (2009). Apart from this, we obtain the same result (here in presence of a β effect), namely that a cyclone evolving in a cyclonic shear preserves its shape, whereas this is not the case in an anticyclonic shear.

Figure 7c shows the relative amplitude of the anticyclone compared to the cyclone as a function of time: in C, the ratio remains lower than 0.5 whereas it reaches 0.8 in A. This is consistent with Fig. 6e, which shows a coherent vortex dipole at 30 h in A and not in C (Fig. 6b). As in section 3, there is still a correlation between the cyclone stretching and the anticyclone strength, as can be seen by comparing Figs. 7a and 7c. However, the relative amplitude of the anticyclone compared to the cyclone is stronger in A than in C before 34 h (Fig. 7c)—that is, at a time for which the two cyclones still have the same stretching. It can be interpreted as follows. The tilt of the stretched cyclone in A (equal to $-40°$; see Fig. 7b) is more favorable for the anticyclone intensification than the one in C (close to $-90°$) following the results of section 3.

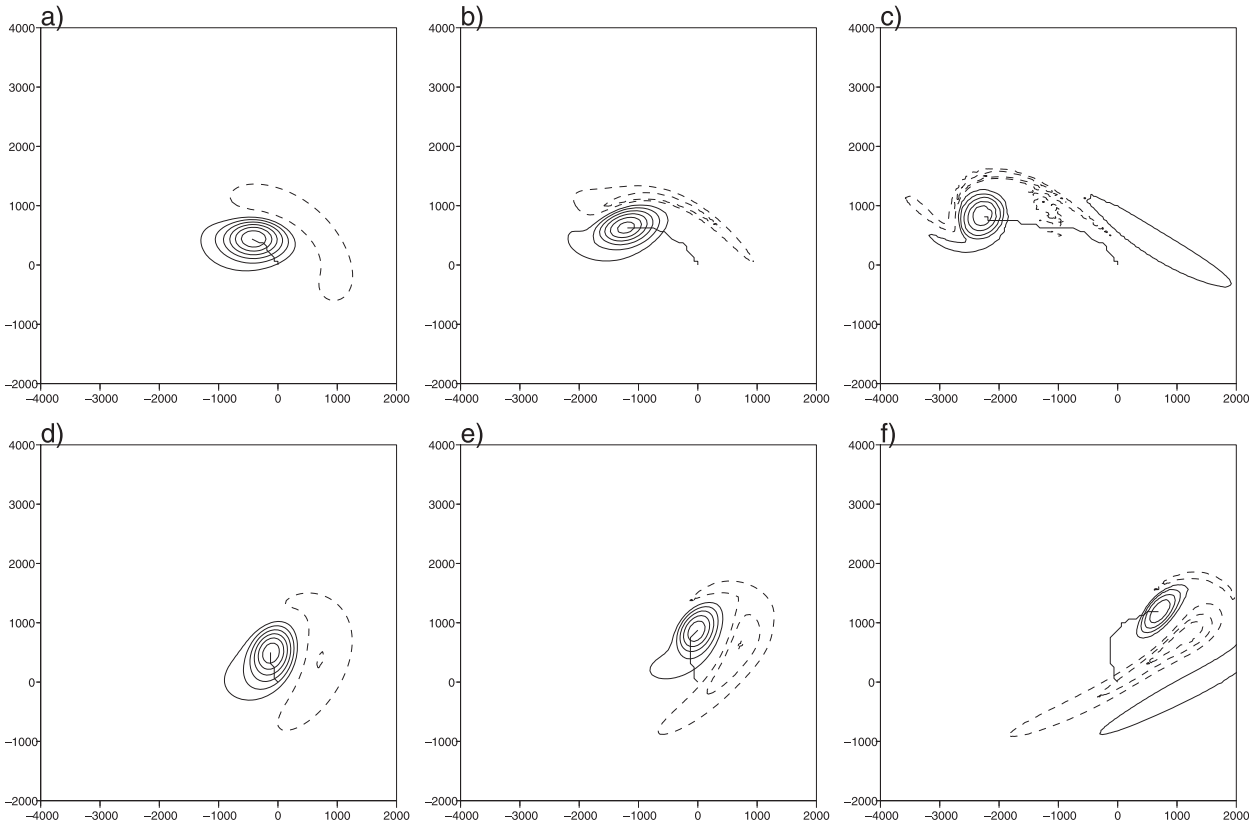

FIG. 6. Relative vorticity field at different times for a cyclone embedded in (a)–(c) a cyclonic shear with $c_x = 0$, $c_y = +0.5$ and (d)–(f) an anticyclonic shear $c_x = 0$, $c_y = -0.5$, at (a),(d) $t = 15$ h, (b),(e) $t = 30$ h, (c),(f) $t = 51$ h. Positive values are represented by solid contours between 2×10^{-5} and 1.1×10^{-4} s^{-1} every 1.8×10^{-5} s^{-1}. Negative values are represented by dashed contours between -1.1×10^{-4} and -2×10^{-5} s^{-1} every 1.8×10^{-5} s^{-1}. The thick black line is the trajectory of the cyclone.

The different relative positions of the anticyclone around the cyclone in C and A are due to the fact that the cyclone advects the weaker anticyclone around it, and this rotation is cyclonic. However, the anticyclone motion is sensitive to the sign of the background shear. In A, these two effects tend to compensate each other so that the anticyclone remains almost constantly to the east of the cyclone. On the contrary, in C these two effects add up to each other so that the anticyclone turns rapidly around the cyclone. This is confirmed by Fig. 7d, which shows that the angle formed by the vector linking the anticyclone and the cyclone with respect to the x axis (denoted θ; see Fig. 1b) remains almost constant with time in A, whereas it keeps increasing in C. This is also observed in Fig. 6 and was verified with other values of c_y (not shown).

Figure 7e represents the meridional position of the cyclone as function of time for both shears. The cyclone in A moves northward more quickly than the cyclone in C. For instance, at 51 h, the more stretched cyclone, whose aspect ratio equals to 2, is 375 km farther north than the quasi-axisymmetric one (with aspect ratio close to 1.0). This result is consistent with the strength and the position of the anticyclone. In particular, the first differences in meridional positions occur at 12 h (Fig. 7e), just at the moment when differences in anticyclone strength first appear (Fig. 7c). The interpretation of the differences in northward motion is the following. A weaker anticyclone leads to a slower propagation but the position of the anticyclone is also a key factor for the northward motion. Similarly to the case of $\gamma_0 = 45°$ in section 3, the anticyclone in C tends to be displaced to the north of the cyclone and the vortex dipole motion is mostly westward. On the contrary, in A, both the stronger amplitude and the more southeastern position of the anticyclone relative to the cyclone concur to a faster northward motion. According to the results of section 3, a value of γ about $-40°$ is clearly favorable for northward motion.

d. Linearly sheared large-scale flow: The general case

The more general case of $c_x \neq 0$ with $c_y = -0.5$ [see Eq. (10)] is now examined. The effective deformation is

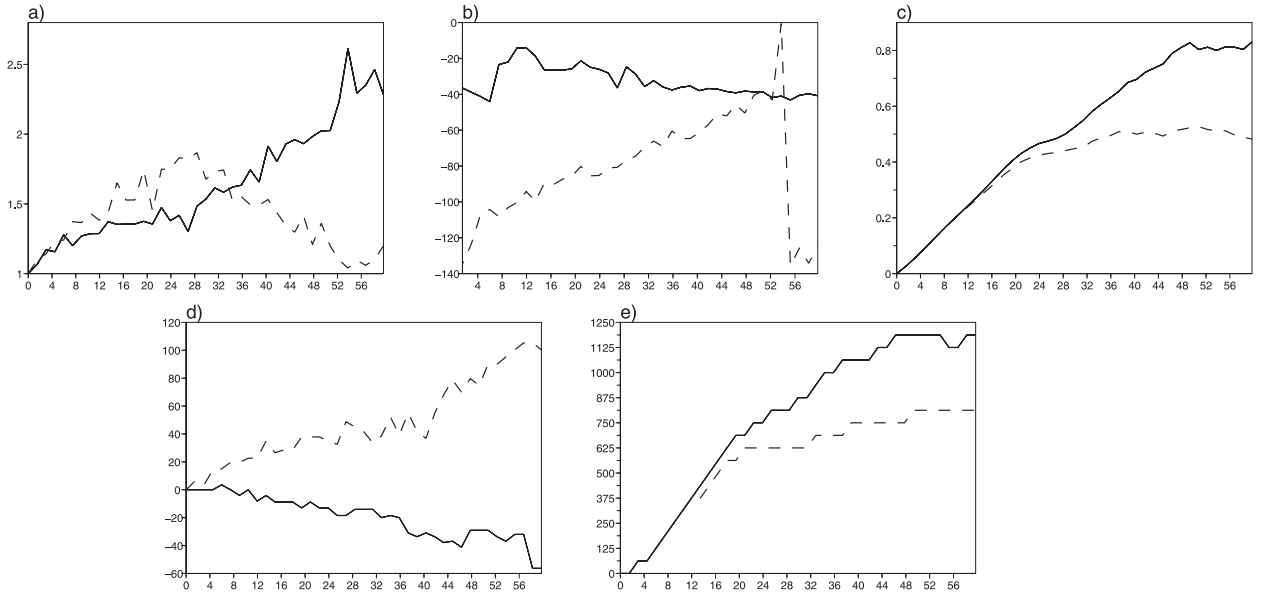

FIG. 7. (a) Cyclone aspect ratio as function of time (h). (b) Cyclone tilt γ (°) as function of time. (c) Ratio of the minimum of the perturbation relative vorticity to its maximum. (d) Angle θ (°). (e) Cyclone's meridional position (km). The solid line represents anticyclonic shear ($c_x = 0$, $c_y = -0.5$); the dashed line represents cyclonic shear ($c_x = 0$, $c_y = 0.5$).

different from zero ($\Delta = -4U^2c_xc_y/a^2$) but (almost) homogeneous in the domain (see the appendix). The flow is dominated by rotation if c_x is negative (Fig. 8a) and dominated by straining if c_x is positive (Fig. 8b). Here, the iso-$\overline{q}$ contours are parallel to the x axis contrary to the background streamlines. This implies that, in addition to the nonlinear term of Eq. (3), the term $\overline{\mathbf{u}} \cdot \nabla q'$ may also be responsible for a northward motion. Therefore, in order to quantify the nonlinear part of the northward motion of cyclones, we must subtract the effect of linear advection. The cyclone position will then be computed by subtracting the cyclone position in the linear experiment to its position in the nonlinear experiment. Note that this method is all the more limited that linear and nonlinear trajectories separate farther apart.

Axisymmetric cyclones with $\max(\zeta') = 1.5 \times 10^{-4}$ s^{-1} and $\max(v') = 22$ m.s^{-1} are introduced at the initial time as before. Cyclones are initialized at the position ($x = -1875$ km, $y = +1875$ km), namely on the bisector in the northwest part of the domain. The reason for choosing this location is that it allows the cyclone in the deformation flow not to move too fast toward the boundaries of the domain where the deformation is not uniform anymore. The streamlines give a flow toward the northeast in the rotation-dominated flow (Fig. 8a) and a flow toward the southeast in the deformation-dominated flow (Fig. 8b). This is not an issue since we correct the motion relative to the linear trajectory. We have checked that other initial conditions give the same qualitative results as soon as they are far from the boundaries (not shown).

As expected, the cyclone evolving in the $\Delta < 0$ flow ($c_x = -0.4$) remains quasi-axisymmetric (Fig. 8a) whereas that in the $\Delta > 0$ flow is deformed and tilted with an angle $\gamma \approx -20°$ with respect to the iso-$\overline{q}$ (Fig. 8b). The stretched cyclone has the stronger anticyclone (Fig. 8b) and its meridional position corrected from linear advection is more to the north (the corrected meridional position is 937.5 km against 1125 km at 35.8 h), consistent with previous results.

Figure 9 shows the results of simulations at $t = 35.8$ h for which $c_y = -0.5$ and c_x varies from 0 to 0.5 (corresponding to cases dominated by strain) and from -0.5 to 0 (corresponding to cases dominated by rotation). First, we observe a correlation between the aspect ratio of the cyclone (Fig. 9a) and $\Delta = -4U^2c_xc_y/a^2$ for the cases of positive Δ ($c_x > 0$), as expected from the results of Kida (1981). When the effective deformation is negative ($c_x < 0$), the aspect ratio stays close to 1.

Figure 9b represents the tilt γ (see Fig. 1) for various values of c_x. For $c_x > 0$, γ is close to $-20°$ whereas for $c_x < 0$, the tilt keeps decreasing when $|c_x|$ increases. This can be interpreted as follows: for $c_x > 0$, the cyclone deforms along a direction close to that of the dilatation axis ($\gamma = -45°$) due to linear terms, but since the self-rotation of the cyclone is cyclonic, its orientation turns closer to the PV gradient, and γ becomes closer to $-20°$. On the contrary, for $c_x < 0$, the vorticity of the ambient flow $\overline{\zeta} = U(c_x + c_y)/a$ is strongly negative because

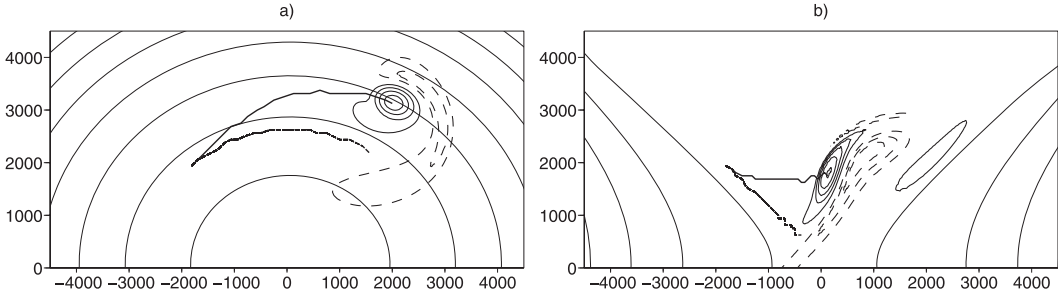

FIG. 8. Relative vorticity field at $t = 35.8$ h. (a) Negative effective deformation ($c_x = -0.4$ $c_y = -0.5$) and (b) positive effective deformation ($c_x = 0.4$, $c_y = -0.5$). Positive values are represented by solid contours between 2×10^{-5} and 10×10^{-5} s^{-1} every 2×10^{-5} s^{-1}. Negative values are represented by dashed contours between -10×10^{-5} and -2×10^{-5} s^{-1} every 2×10^{-5} s^{-1}. The thick line represents the trajectory of the perturbation (dashed line for linear evolution, solid line for nonlinear evolution); the thin line represents iso-$\overline{\psi}$.

$c_y = -0.5$. This means that the background flow exerts an anticyclonic rotation on the cyclone, all the more important when c_x approaches -0.5. This explains why γ becomes more negative when c_x tends to -0.5 in the rotation-dominated flow (Fig. 9b).

The anticyclone is weaker for $c_x < 0$ than for $c_x > 0$ (Fig. 9c), which is logical because the latter case has a more favorable orientation $\gamma \approx -20°$ for the anticyclone formation according to section 3.

Let us look at the position of the anticyclone around the cyclone (Fig. 9d). In the rotation-dominated flow, for moderate negative values of c_x, the anticyclone is located to the southeast of the cyclones, and for strong negative values it is mostly to the east. Around $c_x = -0.25$, a rapid change of tendency can be observed. A detailed examination of the time evolution (not shown) has led to the following interpretation: for strong negative values of c_x, the anticyclone seems to move closer to the cyclone (a possible explanation could be related to the large-scale flow). In that case, we can expect that the anticyclone will also wrap up around the cyclone more rapidly (by comparison with cases of moderate negative values of c_x). As a result, the anticyclone moves to the east-northeast of the cyclone, a favorable location for its growth through the beta effect. On the contrary, for moderate negative values of c_x, the anticyclone remains southeast of the cyclone and does not amplify. This is also in agreement with Fig. 9c. In the deformation-dominated flow, as c_x

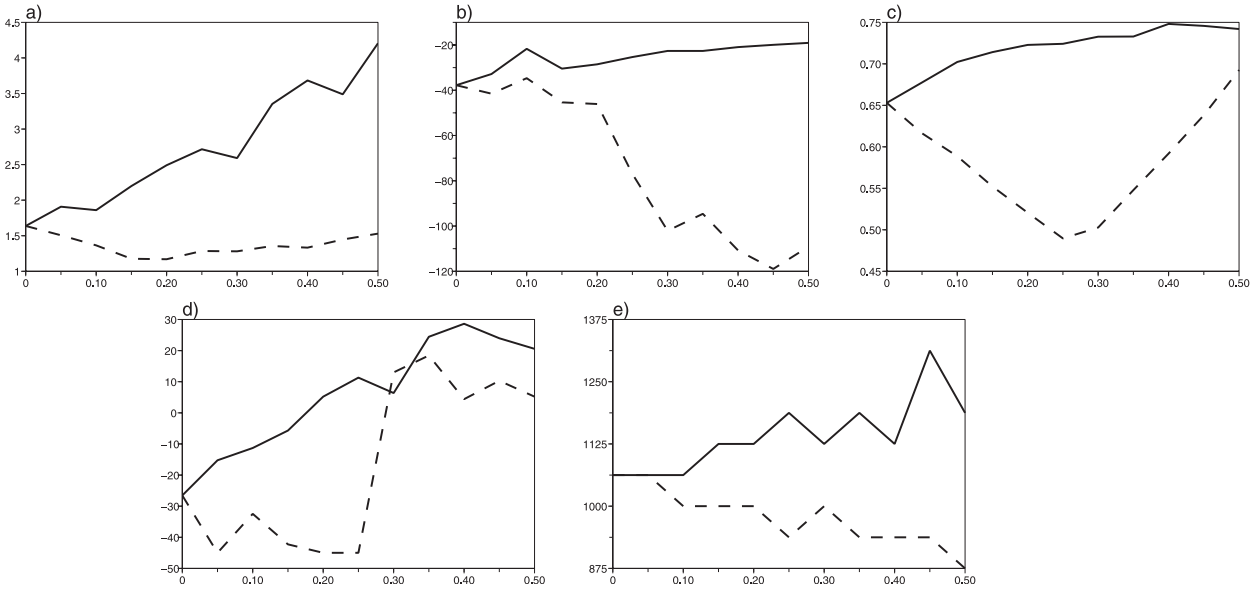

FIG. 9. (a) Cyclone aspect ratio for different c_x (abscissa represents $|c_x|$). (b) Cyclone tilt γ (°) as a function of time. (c) Ratio of the minimum of the perturbation relative vorticity to its maximum. (d) Angle θ (°). (e) Cyclone's meridional position corrected from linear advection (km). The solid line represents positive effective deformation ($c_x > 0$, $c_y = -0.5$); the dashed line represents negative effective deformation ($c_x < 0$, $c_y = -0.5$). The different quantities are computed at 35.8 h.

increases from 0 to 0.5, the anticyclone tends to move to the northeast of the cyclone. It is in agreement with the explanation given for the position of the anticyclone in the case of linearly sheared zonal flow. Indeed, as c_x becomes more positive, the background flow has a weaker anticyclonic rotation, which is less able to counteract the advection by the cyclone.

Finally, Fig. 9e represents the meridional position of the cyclone corrected from its linear trend. It is clear that the cyclone in a deformation-dominated flow ($\Delta > 0$ and $c_x > 0$) moves farther northward than a cyclone in a rotation-dominated flow. A correlation is observed among the aspect ratio of the cyclone (Fig. 9a), the anticyclone strength (Fig. 9c), and the meridional position of the cyclone (Fig. 9e). The more northward motion for the deformation-dominated flow can be also explained by the more favorable orientation of the vortex, as already said (Fig. 9b), and the main eastward position of the anticyclone relative to the cyclone (Fig. 9d).

These results have been checked to be qualitatively the same using an initially shielded vortex (i.e., with an anticyclonic ring such that the total vorticity integrated over the domain is zero). In that case, the same mechanisms are at play, but the anticyclone is much stronger on the eastern side of the cyclone (as the negative vorticity ring rearranges itself on the western and eastern side of the cyclone). The difference in beta drift was therefore amplified in that case.

5. The general case of a meandering large-scale jet

a. The experimental design

The last two sections have highlighted the role of the stretching and nonlinearities in the meridional motion of a cyclone. We now examine a spatially nonuniform jet that is meandering, a situation more realistic for the atmosphere. Gilet et al. (2009) have studied the time evolution of a cyclone in a purely zonal jet (i.e., with no effective deformation) and have shown that the cyclone trajectory was dependent on the shear and the beta effect. To take into account a flow with a nonzero effective deformation, we consider a westerly meandering jet whose streamfunction is defined by

$$\overline{\psi} = -\frac{u_0\sqrt{\pi}}{2\alpha}\,\mathrm{erf}\{\alpha[y - \epsilon\sin(kx - \pi/4)]\}, \quad (11)$$

where $\mathrm{erf}\{l\} = (2/\sqrt{\pi})\int_0^l \exp(-t^2)\,dt$. The wind field can be written as

$$\overline{u} = u_0 \exp(-\{\alpha[y - \epsilon\sin(kx - \pi/4)]\}^2),$$
$$\overline{v} = u_0\epsilon k\cos(kx - \pi/4)\exp(-\{\alpha[y - \epsilon\sin(kx - \pi/4)]\}^2). \quad (12)$$

TABLE 1. Parameters of the large-scale meandering westerly jet [see Eq. (11)].

u_0	37.5 m s^{-1}
k	$\frac{4\pi}{L_x} \simeq 8\times10^{-7}$ m^{-1}
ϵ	$\frac{L_y}{4\pi} \simeq 640$ km
α	$\frac{2\pi}{L_y} \simeq 8\times10^{-7}$ m^{-1}
β	1.6×10^{-11} m^{-1} s^{-1}

Table 1 gathers the values of the jet parameters. The size of the domain is now $L_x = 16\,000$ km, $L_y = 8000$ km. The jet maximum (or jet core) is defined as the maximum zonal wind speed whose isoline satisfies $y = \epsilon a\sin(kx - \pi/4)$.

Figure 10 shows the background streamlines, the background PV contours, and the effective deformation as defined in Eq. (9). It can be noted that streamlines and PV contours are not exactly parallel with the latter undulating more than the former. Moreover, the PV gradient $\nabla\overline{q}$ is not spatially uniform anymore, but points mainly northward with a maximum value equal to 7.4×10^{-11} m^{-1} s^{-1}. The effective deformation exhibits positive areas on the northern side of the ridges and on the southern side of the troughs. The relative vorticity field is positive north of the jet (reflecting cyclonic shear) and negative south (reflecting anticyclonic shear); it reaches values on the order of 3.5×10^{-5} s^{-1}. It can be easily shown from Eq. (12) that areas located south of the jet where $\Delta < 0$ (see Fig. 10) correspond locally to cases of section 4c where $c_x < 0$ and $c_y < 0$ and those where $\Delta > 0$ with cases where $c_x > 0$ and $c_y < 0$.

b. Evolution of two cases

The time evolution of two typical cyclones is first described. The numerical simulations were integrated using a spatial resolution of $\Delta x = \Delta y = 62.5$ km and a temporal resolution of $\Delta T = 112$ s.

Figure 11 shows the perturbation relative vorticity for two simulations initialized with a cyclone located at 750 km south of the jet core in a region of negative Δ (Figs. 11a,c,e) and in a region of positive Δ (Figs 11b,d,f). At $t = 16.5$ h, the cyclone initialized in the area where $\Delta < 0$ is still quasi-isotropic (Fig. 11c) whereas the cyclone initialized in the area where $\Delta > 0$ is deformed and tilted with an angle γ near $-20°$ with respect to the local iso-$\overline{q}$ (Fig. 11d). The anticyclone that develops east of the cyclone is visible; at this time its strength is similar in amplitude for the two cases. The less deformed cyclone crosses the jet core in a zone (Fig. 11e) that will appear to be a preferential zone for the jet crossing (see

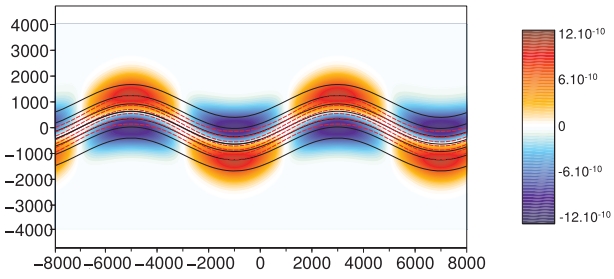

FIG. 10. The color shading is the effective deformation field of the westerly meandering jet. Black contours are the associated streamlines $\overline{\psi}$ and red dashed contours the iso-$\overline{q}$ lines.

following section) and a few hours after the most deformed cyclone that crosses the jet core downstream of the preferential zone (Fig. 11f). Note that the anticyclone is stronger at $t = 24$ h for the deformed cyclone than at $t = 31$ h for the less deformed one. Thus, the most deformed cyclone has a stronger anticyclone and crosses the jet faster than the less deformed one.

To see the robustness of these results, we changed the cyclone radial profile, its amplitude, or its diameter. In these different cases, we qualitatively obtain the same results, except that the stretching of the cyclone may be different, as well as the anticyclone strength, leading to slower or faster northward motion depending on the value of these parameters.

c. *Statistical study of cyclones characteristics*

The model is successively initialized with 256 cyclones located in the 256 grid points along the x axis, at a distance d to the south of the jet core, d varying from 375 to 1000 km every 125 km. It leads to $256 \times 6 = 1536$ trajectories.

Statistics on the 1536 cyclones are analyzed in the present section to confirm the mechanisms leading to the northward motion of the cyclones. The trajectory is defined as the successive positions of the maximum of the perturbation relative vorticity field as a function of time. We arranged it so that we always consider the main cyclone: indeed, dispersion of Rossby waves leads to the growth of a secondary cyclone which can become stronger than the main cyclone after some time. Other ways of tracking the cyclone consist in considering either the minimum of perturbation streamfunction field or the northeastern point of a given isoline of relative vorticity [e.g., $\zeta' = 0.8 \max(\zeta')$]. These two last methods led to similar results as the first one.

The position and time of the jet crossing is defined as follows. For each cyclone trajectory, the crossing point, noted (x_c, y_c), is estimated by finding time t_a such that $[x(t_a - \Delta T_{st}), y(t_a - \Delta T_{st})]$ and $[x(t_a), y(t_a)]$, are on the anticyclonic and cyclonic side of the jet, respectively ($\Delta T_{st} = 1.5$ h corresponds to the time for data storage). The values x_c, y_c, and the corresponding time t_c are then computed by linear interpolation. This last estimation reveals to be sufficient to obtain satisfactory results.

Figure 12a is a scatterplot of the average aspect ratio of cyclones between $t = 0$ and 18 h as a function of Δ integrated along their trajectory between 0 and 18 h. The symbols are associated with different initial distances of cyclones to the jet core. There exists a clear correlation between the stretching of cyclones and the effective deformation of the large-scale jet integrated along their trajectory, as can be expected.

Let us now look at the anticyclones which develop east of the main cyclones. Figure 12b shows the scatterplot of the ratio of the absolute value of the relative vorticity minimum to its maximum at $t = 18$ h versus the average aspect ratio of cyclones between $t = 0$ and 18 h. For cyclones too far away from the jet center ($d = 875$, 1000 km), the weak PV gradient at this distance prevents the formation of a strong anticyclone by Rossby wave radiation. On the contrary, cyclones close to the jet center ($d = 375$, 500 km) possess very intense anticyclones, as these anticyclones could grow favorably within a large PV gradient. At the same time, these cyclones do not stay enough time in the different regions of deformation to differ from each other because they cross the jet quite rapidly. This is the reason why they have small and similar aspect ratios. For the other sets of distances, a correlation between the cyclone stretching and the anticyclone intensity is verified (see lozenges and diamonds in Fig. 12b).

To quantify the cyclone motion in the direction of the jet core, the cyclone speed component orthogonal to the local iso-$\overline{\psi}$ is introduced and denoted as

$$v_{\perp\overline{\psi}}(t) = -\frac{\mathbf{u}_{\text{traj}}(t) \cdot \nabla\overline{\psi}(t)}{\|\nabla\overline{\psi}(t)\|}, \tag{13}$$

where $\mathbf{u}_{\text{traj}}(t)$ is diagnosed from the cyclone trajectory. To avoid numerical noise when computing this quantity, its average over a time interval is considered:

$$v_{\text{diag}} = \frac{1}{t_2 - t_1} \sum_{t=t_1}^{t_2} v_{\perp\overline{\psi}}(t). \tag{14}$$

Figure 12c represents the scatterplot of v_{diag} between $t_1 = 0$ h and $t_2 = 18$ h versus the ratio of the relative vorticity minimum to its maximum at 18 h. As expected, cyclones having the stronger (weaker) anticyclone have the stronger (weaker) jet crossing speed (correlation coefficient of 0.86 using all cyclones). The velocity toward the jet axis is thus well related to the dipole formed

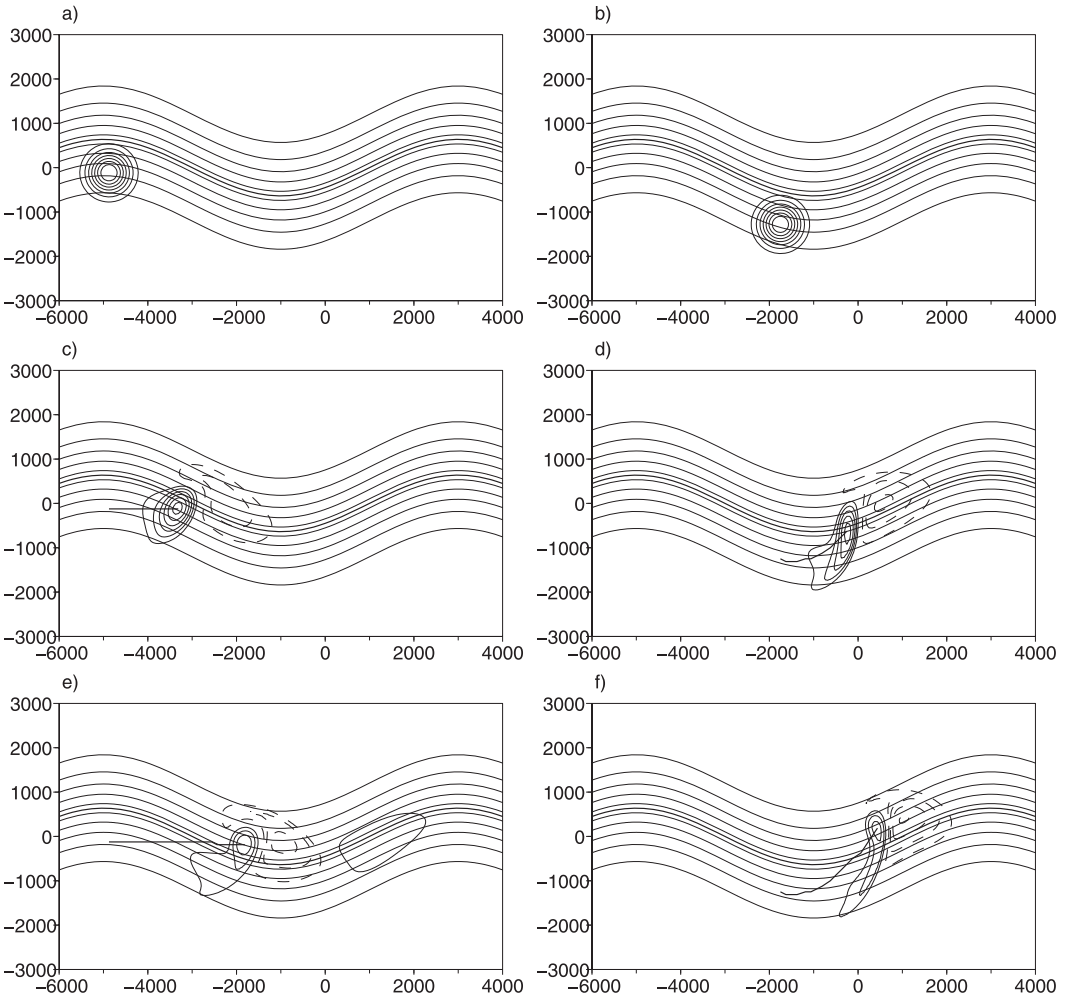

FIG. 11. Black contours indicate the perturbation relative vorticity field for two different initial cyclones at (a),(b) $t = 0$ h; (c),(d) $t = 16.5$ h; and (e) $t = 31$ h and (f) $t = 24$ h, corresponding to the time of jet crossing. Positive values are represented by solid contours between 2×10^{-5} and 12.8×10^{-5} s^{-1} every 1.8×10^{-5} s^{-1}. Negative values are represented by dashed contours between -12.8×10^{-5} and -2×10^{-5} s^{-1} every 1.8×10^{-5} s^{-1}. Black lines indicate the large-scale flow streamfunction (thick line: jet center). The axisymmetric cyclone is initially located at $d = 750$ km, $x_i = -4875$ km for (a),(c),(e) and $d = 750$ km, $x_i = -1750$ km for (b),(d),(f).

by the cyclone and its anticyclonic partner. This correlation is also confirmed when comparing the behavior of each category of cyclones as function of their initial distance to the jet axis. The cyclones close to the jet axis (see the crosses in Fig. 12c) experience a large PV gradient, which gives both strong anticyclones and large velocities. On the contrary, cyclones far away from jet axis (see reverse triangles in Fig. 12c) experience a weak PV gradient, which gives both weak anticyclones and small velocities.

Figure 12d completes the picture by showing the scatterplot of v_{diag} with $t_1 = 0$ h and $t_2 = 18$ h, versus the averaged aspect ratio r between t_1 and t_2. For cyclones with initial distances $d = 500$, 625, and 750 km, a correlation can be observed between velocity toward the jet axis and aspect ratio. For cyclones with initial distances close to the jet axis ($d = 375$ km) or far away from the jet core ($d = 875$, 1000 km), there is a smaller correlation between velocity and aspect ratio. As seen above, this might be due to the direct effect of the PV gradient on the anticyclone growth, with stretching playing a less important role for these distances.

Thus, the correlation between the cyclones stretching, the secondary anticyclone and the cyclones' speed component orthogonal to the local iso-$\overline{\psi}$ that was highlighted in the context of no large-scale jet and linearly sheared large-scale jet is still observed here. The main caveat is that the stretching effect can be of smaller

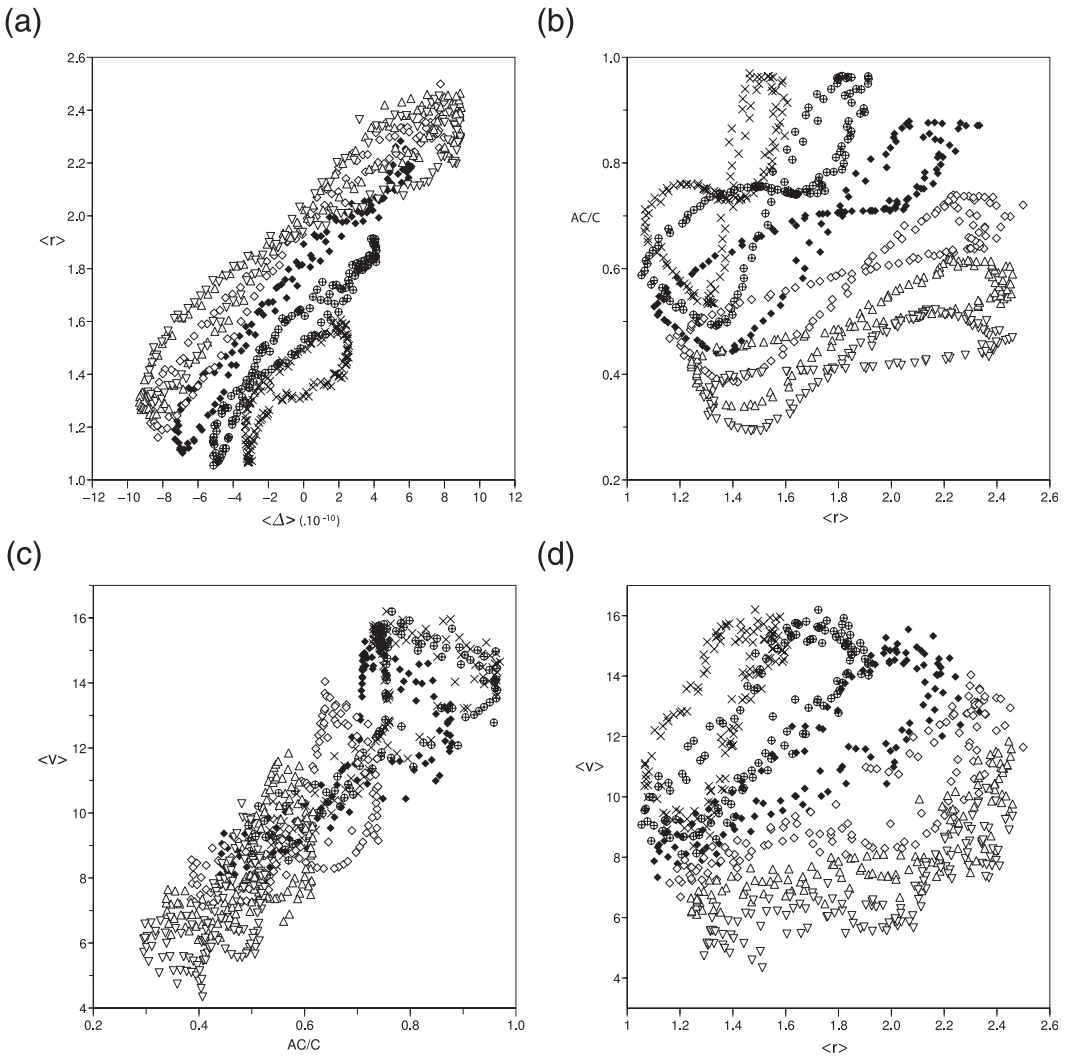

FIG. 12. (a) Scatterplot of the averaged aspect ratio r between 0 and 18 h vs the average of Δ (s^{-2}) between 0 and 18 h (using all cyclones). (b) Scatterplot of the ratio (absolute value) of the minimum of relative vorticity to its maximum at 18 h vs the averaged r between 0 and 18 h. (c) Scatterplot of v_{diag} ($m\,s^{-1}$) between $t_1 = 0$ h and $t_2 = 18$ h vs the ratio of the minimum of relative vorticity to its maximum at 18 h. (d) Scatterplot of v_{diag} ($m\,s^{-1}$) vs the averaged r between 0 and 18 h. Symbols correspond to different initial distances from the jet axis: d = 375 (crosses), 500 (circles), 625 (lozenges), 750 (diamonds), 875 (triangles), and 1000 km (reverse triangles).

importance if the PV gradient of the background flow is too large or too small.

d. *Consequences of deformation mechanisms on the jet-crossing phase*

The mechanisms underlined through the statistical study have highlighted that the motion of the cyclones across the jet axis depends on the deformation field. It may also have an impact on the region of this crossing, as will be examined here.

The histogram of Fig. 13 represents the number of cyclones as function of the zonal position x_c at the time of the jet crossing. The data are gathered by 500-km-wide intervals along the x axis for the 1536 cyclones. The number of cyclones having crossed in each interval is given in percent. The figure shows a preferential zone for the jet-crossing phase, located in the western part of the $\Delta > 0$ area around $x_c = -2000$ km. This result is statistically robust because the value is higher than a uniform distribution value plus its standard deviation.

To understand the existence of this preferential region of crossing, and how it relates to the deformation mechanisms, let us look at the time t_r for which cyclones reach an aspect ratio of 2, as a function of the initial position x_i (Fig. 14, continuous line). For each initial

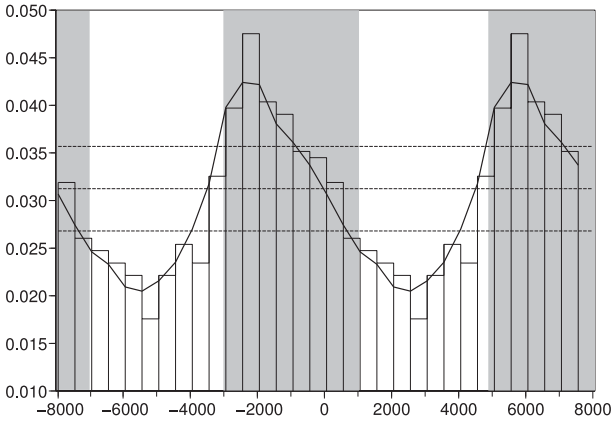

FIG. 13. Histogram of the zonal position x_c at crossing time. The solid line is three-point smoothing. The dashed lines are associated with a random distribution: mean (middle line) and standard deviation added to/subtracted from the mean. Effective deformation $\Delta > 0$ at x_c (south of the jet) in gray shading, and $\Delta < 0$ in white shading.

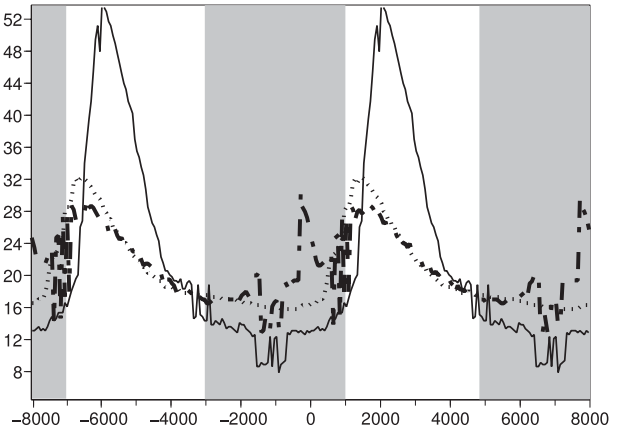

FIG. 14. Crossing time t_c (thick dash-dotted line), t_r (solid line), and t_{ac} (dotted line) (h), as function of the initial longitude of the cyclone x_i (km). Effective deformation $\Delta > 0$ at x_i in gray shading, and $\Delta < 0$ in white shading. Here t_{ac} is the time for which the ratio of the minimum of the perturbation relative vorticity with its maximum reaches 0.55, and t_r is the time when the aspect ratio of the cyclones reaches 2.

distance, the quantity t_r is averaged over the six cyclones initialized with different distances to the jet center. In the rotation-dominated region ($\Delta < 0$), the averaged time is always longer than 20 h, and the longest time is achieved for initial position in the western part of the $\Delta < 0$. In the strain-dominated region $\Delta > 0$, t_r is smaller than 14 h. This is consistent with the correlation between the stretching and the time-integrated effective deformation field (Fig. 12a).

The time of formation of the anticyclone t_{ac} (defined as the time for which the amplitude of the anticyclone is 55% the amplitude of the cyclone) is different between cyclones initialized in $\Delta < 0$ and $\Delta > 0$ regions and is correlated with t_r (cf. the dotted line with the continuous line of Fig. 14). Cyclones initialized in the western part of the rotation-dominated region remain longer in this region than cyclones initialized to the east (not shown). They are therefore less stretched than the others and the formation of their anticyclonic partner is slower.

As can be expected from the statistical results, the time of crossing will be the longest for the cyclones initialized at the western edge of the $\Delta < 0$ area (see the thick dash-dotted line in Fig. 14). On the contrary, cyclones whose t_c is the shortest are those initialized at the western edge of the $\Delta > 0$ area.

Because the time crossing decreases with x_i for negative Δ and for x_i between -7000 and -3000 km (see Fig. 14), cyclones located farther upstream take more time to cross the jet than cyclones located more downstream. This promotes the idea of an accumulation at the crossing time (which is different for each cyclone) of the less stretched cyclones (cyclones initialized in the $\Delta <$ 0 area), which explains the preferential region of the jet crossing located in the western part of the $\Delta > 0$ area (observed in Fig. 13). Indeed, the cyclones which cross the jet in the preferential zone are associated with a slow stretching and a slow growth in time of their anticyclonic partner, which implies that the beta drift is slower for these cyclones. This behavior is to be contrasted with the cyclones that are initialized in the deformation-dominated region. They are stretched very rapidly (see the thin line in Fig. 14 around $x_i = -1000$ km) and their associated anticyclone grows rapidly in time (see the thick line in Fig. 14). The increase in the time crossing with x_i when Δ is positive and x_i is between -300 and 1000 km proves the nonaccumulation of the more stretched cyclones (initialized in the $\Delta > 0$ area) that cross the jet downstream of the preferential zone.

6. Conclusions

We have investigated the role of the horizontal deformation and the nonlinearities on the β-drift motion of a cyclone using a barotropic quasigeostrophic model. Three kinds of simulations were examined: a case with no background flow (for which we examined the influence of the shape of the cyclone on its β drift), a case with a linearly sheared large-scale flow, and a case with a meandering jet.

In the case without any background flow on a β plane, a cyclone moves farther northward as its shape is initially elongated. This effect is all the more pronounced that the tilt of the cyclone with the local potential vorticity isolines is oriented between $-45°$ and 0°. A linear

process assures that a stretching along the meridional direction enhances a secondary anticyclone created by the beta gyres. This cyclone–anticyclone couple then forms a nonlinear vortex dipole that propagates mostly northward.

In a linearly sheared zonal flow, the cyclone evolving in an anticyclonic environment is more stretched and moves northward faster than that embedded in a cyclonic environment. This is consistent with the strength and the position of the secondary anticyclone around the cyclone. This result is a midlatitude extension of the result, obtained in a tropical cyclone context, of Williams and Chan (1994), who showed that an environmental flow with anticyclonic vorticity accelerates the beta drift and a cyclonic vorticity decelerates it.

Experiments with a large-scale flow that includes deformation and vorticity confirm this. Cyclones embedded in a flow dominated by deformation are stretched and move northward more quickly than those in a flow dominated by rotation. This is due to a stronger secondary anticyclone favorably located around the cyclone. Moreover, the more positive the effective deformation is, the faster the beta drift [a result also observed by Li and Wang (1996) in the context of tropical cyclones].

The last part of the paper has dealt with cyclones evolving in a more realistic meandering large-scale flow, whose deformation field is spatially varying. A statistical study revealed a strong correlation among the cyclones stretching, their speed component orthogonal to the streamfunction isolines of the background flow, and the anticyclone strength. These different observations agree with the results obtained with more idealized flows. The deformation mechanisms have consequences on the jet-crossing phase, that is, the phase when a cyclone crosses a jet from its anticyclonic to its cyclonic side. The cyclones initialized in the rotation-dominated region are weakly stretched and move slowly northward. They tend to accumulate slightly to the south of the jet axis at the beginning of a region dominated by the deformation. This region is a preferential zone for the jet crossing. On the contrary, the more stretched cyclones move quickly northward, so that they cross the jet at different locations in space downstream of the preferential zone.

These results can be put in parallel with the study of Vandermeirsh et al. (2003), who examined the interaction between a vortex and a zonal jet in the ocean. They showed that weak vortices (comparing to the rotation of the jet) drift along the jet without crossing it whereas strong ones can cross the jet by forming a dipole with an opposite-signed patch of vorticity or by forming filaments.

The results obtained here suggest that the jet-crossing phase often observed of midlatitude cyclones (Baehr et al. 1999; Rivière and Joly 2006a; Wallace et al. 1988) can be attributed to the combined effects of nonlinearities and deformation in presence of meridional PV gradient due to the existence of the jet. When baroclinic effects are taken into account, it is not the lower-layer PV gradient that matters for the surface cyclone northward motion, but the barotropic meridional PV gradient, as shown by Gilet et al. (2009) in a two-layer quasigeostrophic model in the case of the evolution of a surface cyclone embedded in baroclinic zonal flows. We conjecture by inspecting Fig. 11 of Gilet et al. (2009) that the formation of a strong anticyclone on the eastern side of the cyclone occurs in the upper layer, promoting a vortex dipole that is able to propagate northward and to advect the lower-layer cyclone northward as well. We will examine this mechanism and the energetics of the surface cyclone life cycle in a forthcoming paper.

Acknowledgments. The authors want to acknowledge stimulating discussion with Philippe Arbogast, John Methven, Heini Wernli, and Xavier Carton. GL and LO acknowledge funding by the MAIF foundation through the REVAEE project.

APPENDIX

Description of the Linear Deformation Flow

The large-scale flow described by Eq. (10) corresponds to a uniform relative vorticity field $\bar{\zeta} = (U/a)(c_x + c_y)$. To respect the biperiodicity of the domain, four additive fields were superimposed on the uniform one:

$$\bar{\zeta} = \frac{U}{a}(c_x + c_y) + f_N(y) + f_S(y) + f_E(x) + f_O(x).$$

Each field f is allowed to periodize the domain at each edge (north, south, east, and west).

The profile of $f_s(y)$ is defined as

$$f_S(y) = -\frac{2}{3}\frac{U}{a}c_y\left\{1 + \cos\left[2\pi\frac{(y - y_S)}{l_y}\right]\right\},$$

$$f_S(y) = 0, \quad \text{and} \quad y > y_S - l_y/2$$

with $y_S = 3937.5$ km and $l_y = 6000$ km. This function is therefore zero between -3000 and 4000 km. Defining a similar function for f_N, we then obtain a periodic function for ζ in y. The definitions of f_E and F_O are similar.

REFERENCES

Baehr, C., B. Pouponneau, F. Ayrault, and A. Joly, 1999: Dynamical characterization of the FASTEX cyclogenesis cases. *Quart. J. Roy. Meteor. Soc.,* **125,** 3469–3494.

Bjerknes, J., and H. Solberg, 1922: Life cycle of cyclones and the polar front theory of atmospheric circulation. *Geofys. Publ.,* **3,** 3–18.

Cai, M., and M. Mak, 1990: On the basic dynamics of regional cyclogenesis. *J. Atmos. Sci.,* **47,** 1417–1442.

Davies, H. C., C. Schär, and H. Wernli, 1991: The palette of fronts and cyclones within a baroclinic wave development. *J. Atmos. Sci.,* **48,** 1666–1689.

Dritschel, D. G., 1990: The stability of elliptical vortices in an external straining flow. *J. Fluid Mech.,* **210,** 223–261.

Gilet, J.-B., M. Plu, and G. Rivière, 2009: Nonlinear baroclinic dynamics of a surface cyclone crossing a zonal jet. *J. Atmos. Sci.,* **66,** 3021–3041.

Holland, G. J., 1983: Tropical cyclone motion: Environmental interaction plus a beta effect. *J. Atmos. Sci.,* **40,** 328–342.

James, I., 1987: Suppression of baroclinic instability in horizontally sheared flows. *J. Atmos. Sci.,* **44,** 3710–3720.

Kida, S., 1981: Motion of an elliptic vortex in a uniform shear flow. *J. Phys. Soc. Japan,* **50,** 3517–3520.

Lapeyre, G., P. Klein, and B. Hua, 1999: Does the tracer gradient vector align with the strain eigenvectors in 2D turbulence? *Phys. Fluids,* **11,** 3729–3737.

Legras, B., and D. Dritschel, 1993: Vortex stripping and the generation of high vorticity gradients in two-dimensional flows. *Appl. Sci. Res.,* **51,** 445–455.

Li, X., and B. Wang, 1996: Acceleration of the hurricane beta drift by shear strain rate of an environmental flow. *J. Atmos. Sci.,* **53,** 327–334.

McWilliams, J., and G. Flierl, 1979: On the evolution of isolated, nonlinear vortices. *J. Phys. Oceanogr.,* **9,** 1155–1182.

Okubo, A., 1970: Horizontal dispersion of floatable particles in the vicinity of velocity singularities such as convergences. *Deep-Sea Res.,* **17,** 445–454.

Rivière, G., 2008: Barotropic regeneration of upper-level synoptic disturbances in different configurations of the zonal weather regime. *J. Atmos. Sci.,* **65,** 3159–3178.

——, and A. Joly, 2006a: Role of the low-frequency deformation field on the explosive growth of extratropical cyclones at the jet exit. Part I: Barotropic critical region. *J. Atmos. Sci.,* **63,** 1965–1981.

——, and ——, 2006b: Role of the low-frequency deformation field on the explosive growth of extratropical cyclones at the jet exit. Part II: Baroclinic critical region. *J. Atmos. Sci.,* **63,** 1982–1995.

Schultz, D., D. Keyser, and L. Bosart, 1998: The effect of large-scale flow on low-level frontal structure and evolution in midlatitude cyclones. *Mon. Wea. Rev.,* **126,** 1767–1791.

Shapiro, M., and D. Keyser, 1990: Fronts, jet streams, and the tropopause. *Extratropical Cyclones: The Erik Palmén Memorial Volume,* C. W. Newton and E. O. Holopainen, Eds., Amer. Meteor. Soc., 167–191.

Sutyrin, G., and X. Carton, 2006: Vortex interaction with a zonal Rossby wave in a quasi-geostrophic model. *Dyn. Atmos. Oceans,* **41,** 85–102.

Thorncroft, C. D., B. J. Hoskins, and M. McIntyre, 1993: Two paradigms of baroclinic-wave life-cycle behaviour. *Quart. J. Roy. Meteor. Soc.,* **119,** 17–55.

Trieling, R. R., J. M. A. van Wesenbeeck, and G. J. F. van Heijst, 1998: Dipolar vortices in a strain flow. *Phys. Fluids,* **10,** 144–159.

Uccelini, L. W., 1990: Processes contributing to the rapid development of extratropical cyclones. *Extratropical Cyclones: The Erik Palmén Memorial Volume,* C. W. Newton and E. O. Holopainen, Eds., Amer. Meteor. Soc., 81–105.

Ulrich, W., and R. K. Smith, 1991: A numerical study of tropical cyclone motion using a barotropic model. II: Motion in spatially-varying large-scale flows. *Quart. J. Roy. Meteor. Soc.,* **117,** 107–124.

Vandermeirsh, F., X. Carton, and Y. G. Morel, 2003: Interaction between an eddy and a zonal jet. Part I. One-and-a-half-layer model. *Dyn. Atmos. Oceans,* **36,** 247–270.

Wallace, J., G.-H. Lim, and M. Blackmon, 1988: Relationship between cyclone tracks, anticyclone tracks and baroclinic waveguides. *J. Atmos. Sci.,* **45,** 439–462.

Wang, B., X. Li, and L. Wu, 1997: Direction of hurricane beta drift in horizontally sheared flows. *J. Atmos. Sci.,* **54,** 1462–1471.

Weiss, J., 1991: The dynamics of enstrophy transfer in two-dimensional hydrodynamics. *Physica D,* **48,** 273–294.

Wernli, H., R. Fehlmann, and D. Luthi, 1998: The effect of barotropic shear on upper-level induced cyclogenesis: Semi-geostrophic and primitive equation numerical simulations. *J. Atmos. Sci.,* **55,** 2080–2094.

——, S. Dirren, M. A. Liniger, and M. Zillig, 2002: Dynamical aspects of the life cycle of the winter storm 'Lothar' (24–26 December 1999). *Quart. J. Roy. Meteor. Soc.,* **128,** 405–429.

Williams, R. T., and J. C. L. Chan, 1994: Numerical studies of the beta effect in tropical cyclone motion. Part II: Zonal mean flow effect. *J. Atmos. Sci.,* **51,** 1065–1076.